Density Functional Theory Study of Bulk Properties of Transition Metal Nitrides

Michael Lynn,[1] Damilola Ologunagba,[1] Beni B. Dangi[2*], Shyam Kattel[1*]

[1] *Department of Physics, Florida Agricultural and Mechanical University, Tallahassee, FL 32307*

[2] *Department of Chemistry, Florida Agricultural and Mechanical University, Tallahassee, FL 32307*

Corresponding authors: beni.dangi@famu.edu; shyam.kattel@famu.edu

Abstract

Density functional theory (DFT) calculations are performed to compute the lattice constants, formation energies and vacancy formation energies of transition metal nitrides (TMNs) for transition metals (TM) ranging from 3d-5d series. The results obtained using six different DFT exchange and correlation potentials (LDA, AM05, BLYP, PBE, rPBE, and PBEsol) show that the experimental lattice constants are best predicted by rPBE, while the values obtained using AM05, PBE, rPBE and PBEsol lie between the LDA and BLYP calculated values. A linear relationship is observed between the lattice constants and formation energies with the mean radii of TM and the difference in the electronegativity of TM and N in TMNs, respectively. Our calculated vacancy formation energies, in general, show that N-vacancies are more favorable than TM-vacancies in most TMNs. We observe that N-vacancy formation energies are linearly correlated with the calculated bulk formation energies indicating that TMNs with large negative formation energies are less susceptible to the formation of N-vacancies. Thus, our results from this extensive DFT study not only provide a systematic comparison of various DFT functionals in calculating the properties of TMNs but also serve as reference data for the computation-driven experimental design of materials.

1. Introduction

Transition metal nitrides (TMNs), due to their high electrical conductivity, unique electronic structure, superior chemical stability, and excellent mechanical strength, have generated significant research interest recently and showed great potential for electrochemical energy conversion and storage applications, including as super capacitors, heterogeneous catalysts, and rechargeable batteries.[1-6] Furthermore, metal nitrides offer fabrication and integration advantages due to their high melting temperature, mechanical strength and chemical inertness, which could be useful in integrating them in plasmonics with nanoelectronics.[7-9] Along with transition metal carbides, TMNs are subject to investigation of their various physical and chemical properties.[10-12] Understanding fundamental structural properties such as lattice constants, and defects in crystalline solids is essential for characterizing their thermal, electrical and mechanical behaviors. While limited experimental studies provide some properties such as lattice constants, and bonding parameters;[13, 14] computational first-principles studies have been the main tools for exploring physical and chemical properties of a wide range of TMNs including the investigation of their vacancies formation energies, which provide a deeper insight into the existence of vacancies in TMNs .[2, 15-18]

Density functional theory (DFT) calculations have been widely utilized to study the fundamental properties of TMNs, such as point defect, lattice constant, vacancy formation energy, cohesive energy, and bulk modulus.[10-12, 19-21] However, the accuracy of DFT calculated materials properties depends on the level of treatment of electronic exchange and correlation effects within the DFT approach. In this regard, a comprehensive study that includes the performance of different DFT exchange and correlation functionals is highly useful. Few prior DFT studies have included various DFT functionals to study the bulk properties of metals, metal oxides, and TMNs.[17, 22, 23]

For example, Fuchs *et al.* compared GGA and LDA functionals in predicting the cohesive energies of cubic AlN, GaN, and InN,[17] while Mnsi et al., studied electronic and optical properties of ScN in NaCl-B1, CsCl-B2, ZB-B3 and NiAs-B8 phases.[24] Fuchs *et al*. found that Lattice parameters were described with similar accuracy within the PBE-GGA and LDA while the heats of formation of the group-III nitrides were underestimated by the PBE-GGA and given more accurately by the LDA. Medasani *et. al* found that, for macroscopic properties (lattice constants, cohesive energies and bulk modulus) of metals, the results for revTPSS typically lie between LDA and PBE with a mean absolute percentage deviation of 1.1% and 12.1% from the experimental data for lattice constants and cohesive energies respectively; while the revTPSS predicted higher vacancy formation energies when compared to the four other functionals: PBEsol, LDA, PBE and PW91.[22] Similarly, Stampfl and van de Walle compared LDA and GGA for AlN, GaN, and InN that showed neither method is superior to the other in predicting above mentioned properties.[25] In a further effort to measure the accuracies of LDA and GGA approximations, Hass *et al.* evaluated TPSS against LDA, and PBE.[26] This study concluded that the newer GGA functionals, such as the TPSS in general, lead to improvement over LDA and PBE results. Despite some previous efforts, there is a lack of systematic studies to investigate the bulk properties of a large family of TMNs on a single crystal structure/composition using various flavors of DFT exchange and correlation functionals. To fulfill this fundamental knowledge gap, herein, we carry out a systematic DFT study to calculate select bulk properties (lattice constants, formation energy, and vacation formation energy) of TMNs in rocksalt crystal phase for TMs ranging from 3d to 5d using six commonly used DFT exchange and correlation functionals. We find that the absolute values of bulk properties obtained using LDA, AM05, PBE, rPBE, PBEsol and BLYP are slightly different, however the general trends in variation of bulk properties between various TMNs are found to be

similar. Our results also show that many of TMNs show favorable formation energies, indicating the possibility of their experimental synthesis. Furthermore, our calculations show favorable thermodynamics for the formation of vacancies in several TMNs candidates.

2. Computational Methods

Periodic DFT[27, 28] calculations are performed using the plane wave Vienna *Ab-Initio* Simulation Package (VASP) code.[29, 30] We employ six commonly used DFT exchange and correlations functionals, namely: LDA, AM05, BLYP, PBE, rPBE, and PBEsol, for the calculations of bulk properties reported in this paper. All periodic DFT calculations are carried out using a plane-wave cutoff energy of 400 eV. TMNs containing 3d-5d transition metals in rock salt NaCl phases are modeled. The smallest unit cell used to represent TMNs contains 8 atoms with 4 TM and 4 N atoms. A k-point mesh of 12×12×12 is used for the structure optimization of TMN with 8 atoms per unit cell. All atoms are allowed to relax during geometry optimization until the force on each ion is smaller than 0.01 eV/Å. The formation of bulk-TMN is envisioned as:

$$TM_x + N_y \rightarrow bulk - TM_xN_y$$

where x and y represent the number of TM and N atoms in the NaCl phase of TMN; x = y = 4 for a unit cell containing 8 atoms. Similar to previous approaches,[31-33] formation energy (E_F) is calculated as

$$E_F = E\left(bulk - TM_xN_y\right) - xE(TM) - y/2E(N_2)$$

where $E\left(bulk - TM_xN_y\right)$, $E(TM)$, and $E(N_2)$ are DFT calculated total energies of TMN unit cell in rocksalt phase, single TM atoms in the most favorable bulk phases of TM, and N_2 molecules in a large box of 13Å×14Å×15Å dimensions, respectively. For the calculations of $E(TM)$, TMs are optimized in their most favorable phases.

Vacancy formation energies are calculated using a bigger unit cell containing 64 atoms in which the removal of one TM or N atom creates a vacancy concentration of ~1.6%. Based on our test calculations of k-point convergence, a k-point mesh of 3×3×3 is used for calculations related to a supercell containing 64 atoms. The vacancy formation energy $E_F(TM/N-vacancy)$ is calculated according to the scheme:

$$TM_xN_y \rightarrow TM_{x-1}N_y + TM$$

$$TM_xN_y \rightarrow TM_xN_{y-1} + 1/2N_2$$

Thus, $E_F(TM-vacancy) = E\left(TM_{x-1}N_y\right) + E(TM) - E(TM_xN_y)$ and

$E_F(N-vacancy) = E\left(TM_xN_{y-1}\right) + 1/2E(N_2) - E(TM_xN_y)$

Here, $E(TM_xN_y)$, $E(TM)$, and $E(N_2)$ are total energies of TMN unit cell, TM atoms in their most favorable bulk states, and N_2 molecules in the gas phase, respectively. $E\left(TM_{x-1}N_y\right)$ and $E\left(TM_xN_{y-1}\right)$ are the total energies of unit cell with TM and N vacancy, respectively.

3. Results and Discussion

3.1 Lattice constants. Spin-polarized DFT calculations are performed to calculate lattice constants of TMNs containing 3d-5d transition metals (TMs). Our calculated lattice parameters with six different flavors of exchange and correlations functionals are presented in Table 1. In general, it is observed that the lattice constants are underestimated by LDA and slightly overestimated by BLYP. The underestimation of lattice constants noted in the current study is consistent with previous reports.[34] PBE and rPBE, which represent widely used DFT functionals in material science, heterogeneous catalysis and chemistry communities,[35, 36] predicted lattice parameters are in close agreement with the available experimental values, as shown in Table 1.

Table 1. Calculated lattice constants using various DFT functionals.

	Lattice constant (Å)						
TMN	LDA	AM05	PBEsol	PBE	rPBE	BLYP	Expt.*
ScN	4.38	4.41	4.41	4.45	4.47	4.48	4.44
TiN	4.15	4.18	4.18	4.22	4.24	4.26	4.24
VN	4.03	4.05	4.06	4.10	4.12	4.15	4.14
CrN	3.98	4.01	4.03	4.11	4.15	4.17	4.15
MnN	3.92	4.02	4.03	4.09	4.15	4.14	
FeN	3.93	3.96	3.97	4.06	4.10	4.12	
CoN	3.91	3.94	3.94	3.99	4.02	4.05	
NiN	3.96	3.99	4.00	4.05	4.08	4.10	
CuN	4.06	4.09	4.09	4.15	4.18	4.20	
ZnN	4.17	4.20	4.21	4.26	4.29	4.31	
YN	4.70		4.73	4.77	4.79	4.80	4.58
ZrN	4.47	4.49	4.49	4.53	4.55	4.57	
NbN	4.33	4.34	4.34	4.38	4.40	4.43	4.39
MoN	4.25	4.26	4.27	4.30	4.32	4.36	
TcN	4.21	4.22	4.23	4.27	4.29	4.33	
RuN	4.21	4.22	4.23	4.27	4.29	4.33	
RhN	4.22	4.24	4.25	4.29	4.32	4.36	
PdN	4.29	4.31	4.31	4.37	4.40	4.43	
AgN	4.41	4.44	4.44	4.50	4.53	4.56	
CdN	4.54	4.57	4.57	4.63	4.66	4.68	
HfN	4.42	4.44	4.45	4.48	4.50	4.52	4.52
TaN	4.33	4.34	4.35	4.38	4.40	4.43	4.33
WN	4.27	4.28	4.29	4.32	4.34	4.38	
ReN	4.27	4.27	4.28	4.32	4.34	4.38	
OsN	4.27	4.28	4.29	4.33	4.35	4.40	
IrN	4.30	4.31	4.32	4.36	4.38	4.43	
PtN	4.35	4.37	4.38	4.42	4.45	4.50	
AuN	4.48	4.50	4.51	4.56	4.59	4.63	
HgN	4.62	4.65	4.65	4.71	4.74	4.77	

*taken from references within references [19, 37]

We benchmarked the lattice constants calculated using LDA, AM05, BLYP, PBE, and, PBEsol against the values obtained using the rPBE, which has been shown to reliably reproduce experimental trends of catalytic activity and selectivity and is widely used in the field of material science, chemistry and catalysis.[35, 36] The linear correlations observed in Figure 1 show that all

methods show a similar trend in predicting the lattice constants and benchmark well with the results obtained using the rPBE. Figure 1 clearly shows that the experimental lattice constants lie between the lower limit: predicted by LDA and the upper limit: predicted by BLYP functionals. It is noted that the experimental values are closer to the values predicted using PBE, BLYP and rPBE functionals. In particular, the experimental values almost overlap with the values calculated using the rPBE method. Because of its widespread use and ability to predict experimental lattice constants, all further calculated properties using various functionals are plotted against the rPBE functional in the following discussions.

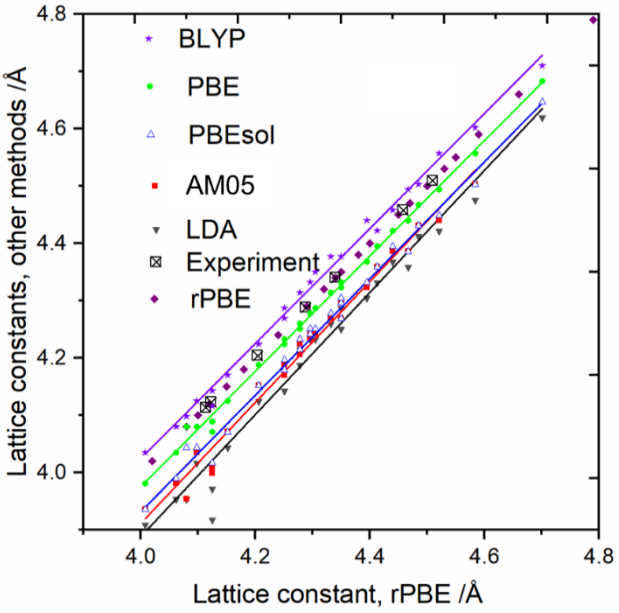

Figure 1. Correlation between lattice constants calculated using LDA, AM05, BLYP, PBE, and, PBEsol with those computed using the rPBE method.

Additionally, DFT-rPBE calculations are performed to compute the lattice constants using 500 eV and 600 eV energy cutoffs as well as van der Waals (DFT-D2 method) and Tkatchenko and Scheffler (T-S) long range corrections. The results show the largest deviation in lattice

constants obtained using 500 and 600 eV energy cutoff and 400 eV-vdW correction vs. 400 eV energy cutoff without vdW correction is less than 4% (Table S1 and Figures S7 and S9 in the supporting information (SI)). This indicates that a 400 eV energy cutoff is a reasonable choice to calculate the lattice constants of TMNs in the rocksalt crystal structure. However, we notice larger deviations in lattice constants values obtained using T-S correction when compared to the values without T-S correction (Table S1 and Figure S8).

Interestingly, we find that the DFT calculated lattice constants show a near-linear correlation with the mean of atomic, ionic, and covalent radii of TMs in TMNs (Figure 2; rPBE values), indicating that the lattice constant of the bulk TMNs in the rock salt structure is primarily determined by the size of TMs present in TMNs. The correlation observed between the DFT calculated lattice constants of TMNs and mean radii of TMs suggests that an advanced machine learning (ML) scheme can be developed to fit the lattice constant with elemental properties of TMs as illustrated in our previous study for the prediction of surface segregation energies given a sizeable DFT dataset of lattice constants are available.[38] Such an ML scheme can utilize elemental properties of TM and N as features to predict the lattice constant as well as the lowest energy bulk phase of binary compounds, including TMNs.

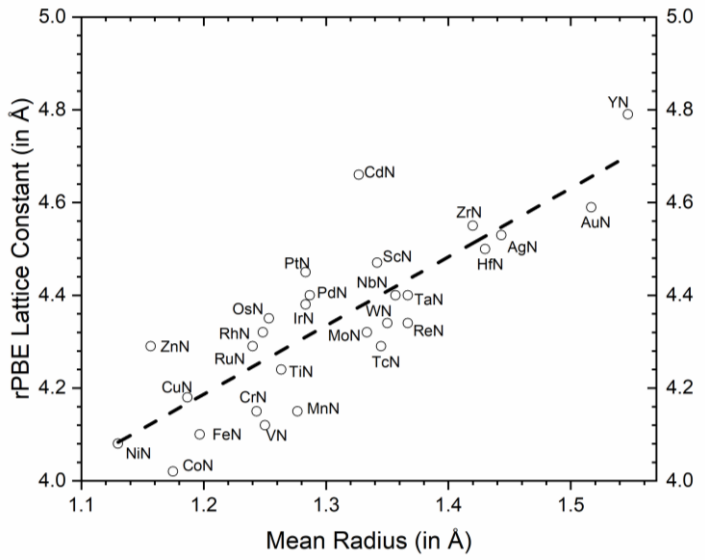

Figure 2. Correlation between the lattice constant of TMNs and mean radii of the corresponding TMs present in TMNs.

3.2 Formation energies of bulk TMNs. The thermodynamic possibility of the formation of bulk TMN phase when TM and N_2 are in close contact can be predicted by computing the formation energies (E_Fs).[10, 31, 39] To this end E_Fs per atom are calculated for all TMNs listed in Table 1 using the method detailed in the computational methods section. The results in Table 2 show negative E_Fs for TMNs: ScN, TiN, VN, CrN, YN, ZrN, NbN, MoN, HfN, and TaN. Our computed negative E_fs indicate that these TMNs thermodynamically prefer to form a bulk TMN rock salt phase due to the reaction of TM with N_2. Importantly, several of these TMNs in the rock salt phase have been experimentally synthesized,[13, 40, 41] validating our theoretical predictions. This demonstrates that DFT screening can be used as an exploratory tool to predict the thermodynamic stability of TMN compounds, answering a key question: do TM and N_2, when mixed, crystallize in the rock salt phase? We note that the formation energies range from ~-2 to ~+2 eV and many TMNs possess E_fs below 1 eV. The relatively moderate E_fs of many of these TMNs suggests that they can be kinetically (such as high-temperature annealing) stabilized in the rock salt cubic phase. The

periodic trends of the computed values show the least stable TMN structures around the middle of a period, while the more stable structures are those of end elements. A slight increase in E_fs are observed from 3d to 4d to 5d, indicating a decrease in the stability.

Table 2. Calculated formation energies of bulk TMNs using various DFT functionals.

Formation energy (eV)/atom						
TMN	LDA	AM05	PBEsol	PBE	rPBE	BLYP
ScN	-2.24	-1.96	-2.02	-1.83	-1.64	-1.83
TiN	-2.23	-1.98	-2.03	-1.81	-1.62	-1.72
VN	-1.43	-1.20	-1.24	-1.03	-0.85	-0.94
CrN	-0.70	-0.49	-0.53	-0.38	-0.25	-0.34
MnN	-0.36	-0.31	-0.35	-0.23	-0.13	-0.18
FeN	-0.18	0.07	0.04	0.24	0.39	0.31
CoN	0.03	0.23	0.20	0.46	0.63	0.55
NiN	0.27	0.47	0.44	0.61	0.76	0.70
CuN	0.71	0.90	0.86	1.03	1.17	1.12
ZnN	0.39	0.60	0.56	0.73	0.88	0.83
YN	-1.79	0.75	-1.57	-1.37	-1.18	-1.35
ZrN	-2.06	-1.78	-1.83	-1.60	-1.40	-1.50
NbN	-1.38	-6.47	-1.17	-0.94	-0.75	-0.81
MoN	-0.38	-0.16	-0.20	0.02	0.19	0.14
TcN	0.12	0.34	0.31	0.50	0.67	0.60
RuN	0.61	0.81	0.78	0.94	1.09	1.02
RhN	0.63	0.82	0.80	0.95	1.10	1.05
PdN	0.84	1.03	1.00	1.18	1.33	1.31
AgN	0.89	1.38	1.25	1.69	2.13	2.14
CdN	0.95	1.15	1.11	1.28	1.43	1.41
HfN	-2.15	-1.87	-1.91	-1.67	-1.46	-1.54
TaN	-1.26	-1.00	-1.03	-0.80	-0.61	-0.65
WN	-0.09	0.16	0.14	0.36	0.54	0.47
ReN	0.70	0.94	0.91	1.10	1.26	1.18
OsN	1.18	1.40	1.37	1.53	1.69	1.59
IrN	1.23	1.43	1.40	1.55	1.69	1.60
PtN	1.13	1.32	1.30	1.46	1.60	1.57
AuN	1.51	1.69	1.66	1.83	1.97	1.98
HgN	1.48	1.69	1.66	1.91	--	2.26

Figure 3 shows a correlation between E_fs calculated using LDA, AM05, BLYP, PBE, and PBEsol with those computed using the rPBE method. A near-perfect linear correlation is observed

between AM05, BLYP, PBE, PBEsol, and rPBE values other than LDA values. Similar to the trend seen in lattice constant predictions (Figure 1), LDA values represent the lower bound for E_fs. However, rPBE values are found to be the upper bound for E_Fs, a different trend than that observed for lattice constants.

In general, PBE, rPBE, and BLYP values are close to each other. Similarly, AM05, PBEsol, and LDA values are close to each other. The PBE values lie in between the lower bound (LDA) and upper bounds (rPBE). Comparing our data obtained using the PBE method with the same functional calculations for selected TMNs by Pathak and Singh, their values are slightly overestimated (more negative).[19] Since they only computed 8 TMNs constituting group 4, 5, and 6 elements, they found a decrease in stability of TMNs from group 4 to 5 to 6 but were unable to predict periodic trends. We find the most stable structures are for Ti, Zr, and Hf, with slightly increasing E_Fs. The most positive E_F values in 3d, 4d, and 5d series were located for Cu, Ag, and Hg, respectively.

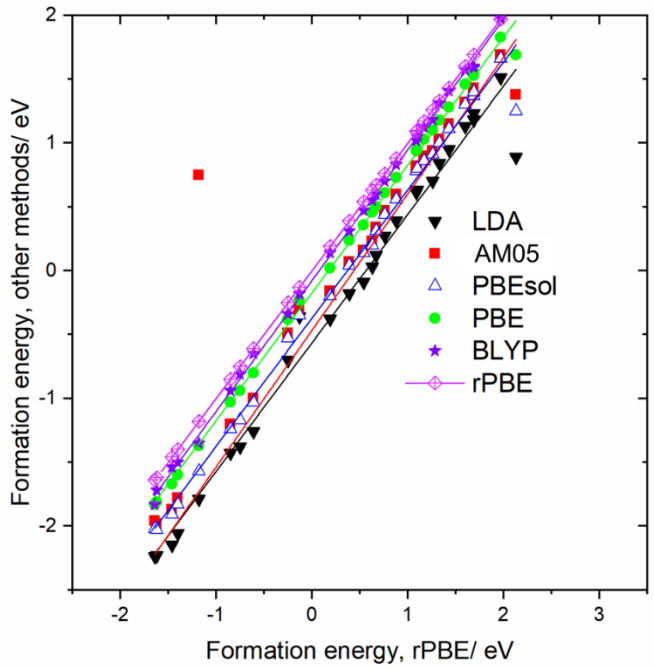

Figure 3. Correlation between the formation energy calculated using LDA, AM05, BLYP, PBE, and, PBEsol with those computed using the rPBE method.

Furthermore, bulk rPBE-TMN E_{Fs} are calculated as a function of TM chemical potential (μ_{TM}). The μ_{TM} ranges from the energy of a TM single atom obtained from DFT calculations of TM single atom in a large box of 13Å×14Å×15Å dimensions to the energy of a TM single atom when optimized in their most favorable bulk phase. The results in Figures S1-S3 in the SI show that bulk TMN formation becomes more favorable when μ_{TM} increases, i. e. when isolated TM atoms are used to form the bulk TMN phase. In addition, E_{Fs} are calculated with vdW and T-S long-range corrections using the rPBE exchange and correlation. The results in Table S2 and Figures S12 and S13 show that the general trends of the values, including the sign of the bulk TMN $E_{Fs,}$ is similar to those calculated without the vdW and T-S corrections. Thus, E_{Fs} calculated without the long-range interaction terms provide a reasonable estimate for the formation of bulk TMNs.

A relationship between the DFT calculated formation energies and an elemental feature is very useful to quickly screen TMN candidates that show favorable thermodynamics using the simple elemental property as a descriptor. We attempted to correlate elemental properties that are readily available (on the web or on a textbook) with our DFT calculated E_fs in Table 2 and find that the E_fs of TMNs correlate well (the deviation from the linear relation is bigger for AgN, CdN, ZnN, WN, MoN and TiN) with the difference in electronegativity of TM and N atoms (Figure 4). In general, a large difference in electronegativity between TM and N (e. g. ScN, HfN, TiN, Yn, ZrN, NbN, TaN, VN) facilitates the formation of bulk TMN in the rock salt phase, as indicated by the large negative E_fs in Figure 4. In contrast, a small difference in electronegativity observed for AuN, AgN, PtN, and IrN shows positive E_fs, indicating unfavorable thermodynamics of these TMN in the rock salt phase. The large electronegativity difference resulting in the formation of

stable TMNs suggests an ionic nature of binding between TMs and N as suggested by previous experimental studies.[42, 43] A closer look at these data helps to derive periodic trends. In each of the 3d, 4d, and 5d periods, with the clear exception of completely filled *nd* orbital elements Zn, Cd & Hg, increasing atomic number leads to the decreasing electronegativity difference and more positive E_fs. In conclusion, based on our calculated E_fs, at least group 3, 4 and 5 elements form stable TMNs in the rock salt structure.

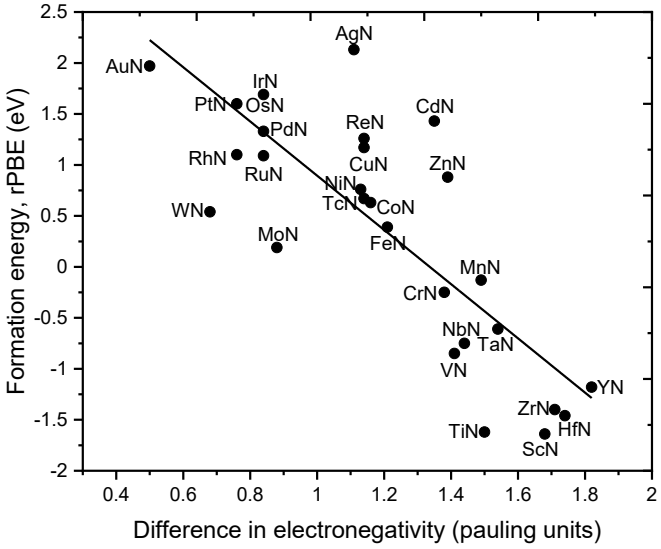

Figure 4. Correlation between DFT calculated formation energies of TMN and the difference in electronegativity of TM and N.

3.3 Vacancy formation energies

3.3.1 Nitrogen and TM vacancy formation energies.

Defects are common in materials. Among various defects, vacancies are the most abundant.[44] To investigate the possibility of vacancy formation in bulk TMNs, one N/TM atom is removed to create a N/TM vacancy in TMN unit cell. Using the approach described in the computational methods section, we calculated the formation energy of N vacancy and TM vacancy

on all TMNs included in this study using LDA, AM05, BLYP, PBE, PBEsol and rPBE functionals. The calculated vacancy formation energy presented in Table 3 shows that, in general, N-vacancy formation is thermodynamically more favorable compared to the formation of TM-vacancy. A comparison of rPBE calculated N and TM vacancy formation energies in Figure 5 shows that N-vacancies are thermodynamically more favorable compared to TM-vacancies; however noted, an opposite trend for NbM, MoN, TcN, TaN, WN, RuN, OsN, IrN, and PtN. Importantly, the general trend of negative formation energies of N-vacancy suggests that such vacancies are expected in bulk TMNs, mostly for 5d and 4d. In fact, the existence of N-vacancies and their role on promoting the electrochemical reactions such as hydrogen evolution reaction and nitrogen reduction reactions have been reported experimentally.[45-48]

Table 3. Calculated vacancy formation energies using various DFT functionals.

N-Vacancy (left) and TM-vacancy (right) formation energies (eV)											
TMN	LDA		AM05	PBEsol		PBE		rPBE		BLYP	
ScN	3.60	9.74	--	3.12	9.27	2.82	8.71	2.47	8.31	2.75	8.09
TiN	2.73	3.95	2.14	2.24	3.55	1.89	3.07	1.56	2.82	1.74	2.48
VN	1.36	1.31	0.82	0.92	1.05	0.60	0.73	0.25	0.58	0.44	0.39
CrN	0.84	0.07	0.35	0.44	-1.01	-1.91	0.23	0.64	0.99	-1.84	0.52
MnN	-0.74	-0.74	0.27	0.36	0.83	0.05	0.54	-0.08	0.53	-0.15	0.16
FeN	0.33	0.22	-0.80	0.16	0.72	-0.43	0.27	-1.39	-0.44	-0.97	-0.10
CoN	-1.20	-0.59	-1.60	-1.55	-0.66	-1.87	-0.99	-2.23	-1.17	-2.03	-1.21
NiN	-0.98	0.95	-1.36	-1.27	0.87	-1.63	0.64	-1.93	0.52	-1.87	0.34
CuN	-1.70	0.91	-2.18	-2.10	0.78	-2.54	0.57	-2.95	0.39	-3.04	0.16
ZnN	-2.59	3.23	-3.02	-2.93	3.08	-3.53	2.69	-3.92	2.49	-4.19	2.12
YN	2.64		--	2.26	7.63	1.98	6.91	1.63	6.52	1.99	6.43
ZrN	3.57	3.63	2.95	3.07	3.24	2.65	2.52	2.25	2.13	2.51	1.58
NbN	1.12	-0.07	0.54	0.59	-0.39	0.01	-0.92	-0.43	-1.20	-0.45	-1.60
MoN	-1.15	-2.11	-1.65	-1.56	-2.31	-2.07	-2.73	-2.43	-2.92	-2.47	-3.27
TcN	-1.62	-3.89	-2.08	-2.02	-4.21	-2.78	-4.93	-3.31	-5.46	-3.66	-5.81
RuN	-4.60	-5.82	-5.23	-4.96	-5.95	-5.41	-6.34	-5.85	-6.59	-5.04	-6.97
RhN	-2.56	-2.61	-3.01	-2.96	-2.86	-3.29	-3.20	-3.62	-3.46	-3.43	-3.46
PdN	-2.27	-0.64	-2.73	-2.57	-0.71	-2.99	-0.97	-3.33	-1.14	-3.29	-1.31
AgN	-3.47	0.38	-4.02	-3.85	-0.12	-4.44	-0.97	-4.94	-1.82	-5.04	-2.16
CdN	-3.52	2.33	-4.09	-3.94	2.16	-4.65	1.63	-5.18	1.28	-5.30	0.89
HfN	3.99	2.97	3.39	3.53	2.60	2.98	1.78	3.43	1.41	2.74	0.74
TaN	0.26	-1.61	-0.31	-0.31	-1.95	-0.97	-2.53	-1.43	-2.82	-1.63	-3.31
WN	-2.33	-4.23	-2.83	-2.84	-4.50	-3.39	-4.93	-3.83	-5.18	-4.02	-5.60
ReN	-12.12	-9.66	-13.35	-13.54	-10.39	-31.28		-17.10	-12.41	-18.84	-13.07
OsN	-7.51	-11.70	-8.29	-8.37	-12.54	-9.70	-13.75	-10.52	-14.39	-11.22	-14.89
IrN	-4.80	-7.91	-5.60	-2.08	-8.53	-6.98	-9.23	-7.79	-9.67	-7.86	-10.08
PtN	-2.34	-3.32	-2.78	-2.71	-3.45	-3.17	-3.78	-3.44	-3.90	-3.50	-4.13
AuN	-4.63	-4.20	-5.10	-4.95	-4.32	-6.46	-4.76	-7.14	-5.18	-7.63	-5.62
HgN	-5.53	-1.37	-6.35	-6.07	-1.68	-7.00	-2.82	-5.31	-0.31	-8.22	-4.34

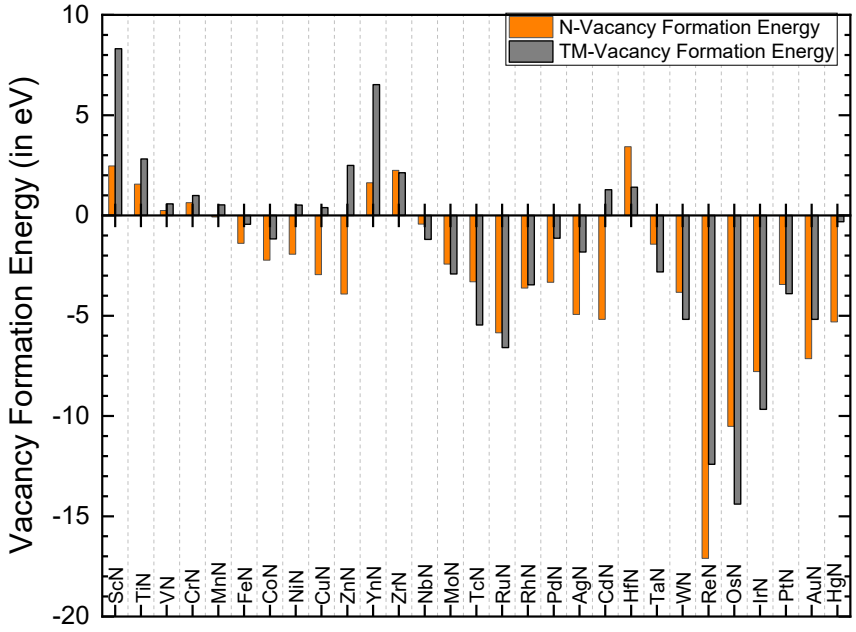

Figure 5. rPBE calculated formation energies of N-vac and TM-vac.

Figure 6 shows the relationship between vacancies formation energies calculated using LDA, AM05, BLYP, PBE, and PBEsol against rPBE values. In general, N-vacancy formation energies decrease in a series with increasing atomic number and decrease from 3d to 4d to 5d series; with a dip at the middle of a series which becomes more prominent from 3d to 4d to 5d. While the dip at Cr is barely clear (only PBE and BLYP functionals), it becomes minima for 4d series at Ru. Linear fits to the data obtained by different functionals show somewhat similar dispersion against rPBE; highest for PBEsol ($R^2 = 0.93$), and lowest for AM05 ($R^2 = 0.98$). LDA, PBE, and BLYP result in R^2 values of 0.96, 0.95, and 0.97; respectively. Balasubramanian et al. investigated the energetics of point defects in rock salt structure of group 3-6 TMNs using PBE functional.[12] They found many stable rock salt structures with low nitrogen vacancy formation energies between -3.2 to 3.2 eV, comparable to our values. LDA and BLYP calculated values represent the lower and upper bounds for N vacancy formation energies (considering absolute

values), respectively (Figure 6). The PBE values lie nearly in the middle of LDA and BLYP calculated values.

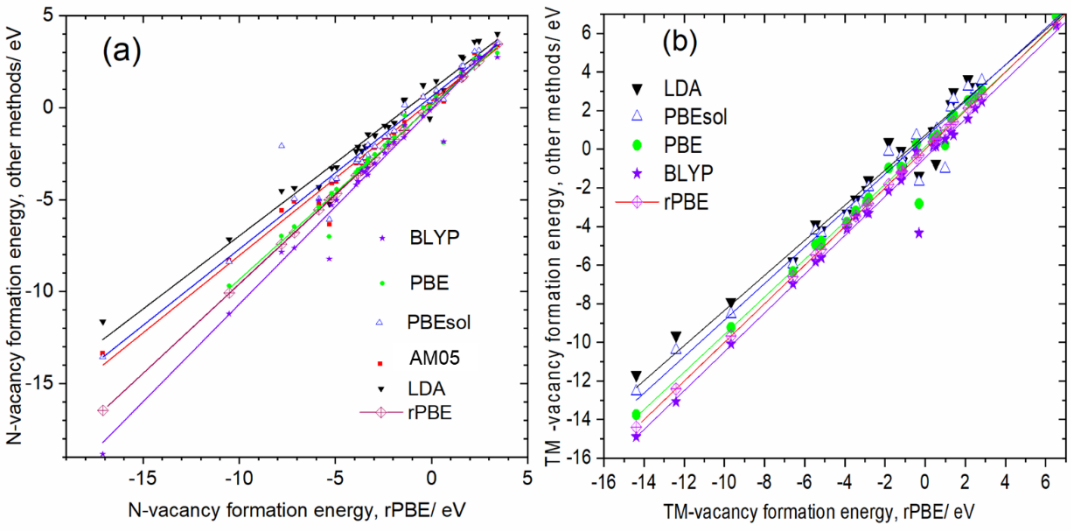

Figure 6. Correlation between (a) N-vacancy and (b) TM vacancy formation formation energy calculated using LDA, AM05, BLYP, PBE, and, PBEsol with those computed using the rPBE method.

The overall trend from 3d to 4d to 5d series indicates a decrease in TM-vacancy formation energies, similar to the N-vacancy formation energies with a minimum at OsN. However, note that the overall spread in TM-vacancy formation energies due to different functionals are relatively small magnitude of 1 to 2 eV which is smaller than the N-vacancy formation energies, especially in the stable regions. Linear fits to the data obtained by different functionals show somewhat similar dispersion against rPBE; highest for LDA (R^2 = 0.96), and lowest for BLYP (R^2 = 0.98). PBEsol and PBE result in R^2 values of 0.97, and 0.98, respectively. TM vacancy formation energy shows a similar trend compared to N vacancy formation energies: LDA: lower bound and BLYP upper bound and PBE between LDA and BLYP values.

We find a linear relationship between the calculated N-vacancy formation energies and E_{FS} (except OsN) of bulk TMNs (Figure 7). TMN candidates that have negative E_{FS} show unfavorable thermodynamics for the formation of N-vacancies. Thus, a higher energy penalty is required to create N- vacancies on TMNs such as ScN, HfN, TiN, ZrN, YN, VN, NbN, TaN, CrN and MnN. In contrast, N-vacancies are predicted to be easily formed on candidates (e. g., OsN, Irn, AgN, and AuN) that have unfavorable thermodynamics of the formation of bulk rock salt phase. The correlation observed in Figure 7 can be used to predict the thermodynamic preference of the formation of N-vacancy using the DFT calculated E_{FS} of bulk TMNs. Such predictions can be used to design TMN candidates with desired properties to guide experiments.

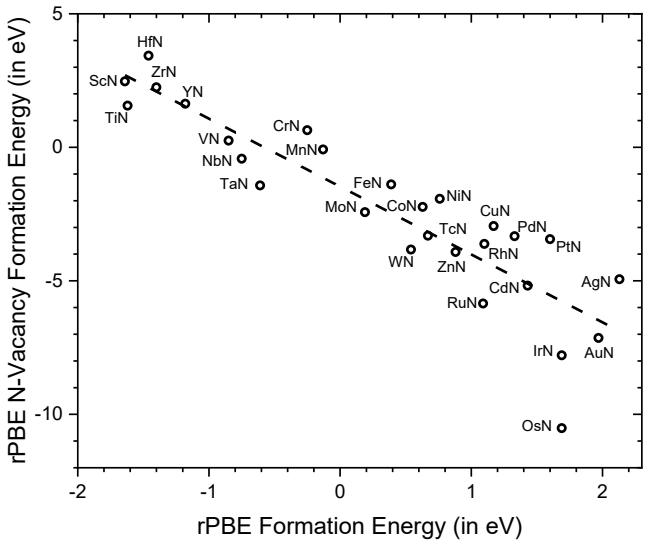

Figure 7. A correlation between formation energy and N-vac formation energy.

Finally, we employed rPBE and modified Becke-Johnson exchange (META-GGA) potentials,[49] to compute the bandgap of TMNs. The META-GGA potentials have been shown to be the best available density functional, closely followed by the HSE06 hybrid functional, to predict the bandgap in a recent study that included extensive benchmarking of 472 solids.[50] The

rPBE and META-GGA calculations predicted that most of the TMNs in rocksalt structures are metallic.

4. Conclusions

In summary, six different DFT functionals are employed to compute bulk properties such as lattice constants, formation energies, and vacancy formation energies of TMNs for TM ranging from 3d-5d. We find that the rPBE calculated lattice constant are found to be very close to the available experimental values. The PBE values for lattice constants, formation and vacancy formation energies represent an average of the LDA, AM05, BLYP, rPBE, and PBEsol calculated values; i. e. the PBE values lie in the middle. The results show that lattice constants and formation energies are linearly correlated with the mean radii of TM and the difference in the electronegativity of TM and N in TMNs, respectively. A large electronegativity difference leads to the formation of thermodynamically stable TMNs in the rock salt phase. Our calculated N-vacancy formation energies indicate that N-vacancies are more favorable than TM-vacancies in most TMNs, indicating a possibility of the occurrence of bulk/surface N-vacancies in TMNs. Furthermore, our results show that N-vacancy formation energies can be expressed as a linear function of the calculated formation energies of bulk TMNs. The linear relationship between N-vacancy formation energies and formation energies implies that TMNs with large negative formation energies are less susceptible to the formation of N-vacancies.

5. Acknowledgements

This work was partially supported by National Science Foundation grants CBET-2200456 and HBCU-UP 2055012. The DFT calculations were performed using computational resources at the Extreme Science and Engineering Discovery Environment, which is supported by the National

Science Foundation Grant number ACI-1548562. BBD acknowledges support from NASA through the NASA Florida Space Grant Consortium (project #006981).

References

1. Z. X. Cheng, W. L. Qi, C. H. Pang, T. Thomas, T. Wu, S. Q. Liu and M. H. Yang, *Adv Funct Mater*, 2021, **31,** 2100553.
2. C. Z. Hu, J. S. Huang, B. G. Sumpter, E. Meletis and T. Dumitrica, *Acs Appl Nano Mater*, 2018, **1**, 2029-2035.
3. R. Qin, P. Y. Wang, C. Lin, F. Cao, J. Y. Zhang, L. Chen and S. C. Mu, *Acta Phys-Chim Sin*, 2021, **37**, 2009099.
4. H. Wang, J. M. Li, K. Li, Y. P. Lin, J. M. Chen, L. J. Gao, V. Nicolosi, X. Xiao and J. M. Lee, *Chem Soc Rev*, 2021, **50**, 1354-1390.
5. W. S. Williams, *Jom-J Min Met Mat S*, 1997, **49**, 38-42.
6. D. Tian, S. R. Denny, K. Z. Li, H. Wang, S. Kattel and J. G. Chen, *Chem Soc Rev*, 2021, **50**, 12338-12376.
7. J. B. Khurgin and A. Boltasseva, *Mrs Bull*, 2012, **37**, 768-779.
8. R. Y. Zhang, X. Y. Li, F. Q. Meng, J. C. Bi, S. D. Zhang, S. Q. Peng, J. Sun, X. M. Wang, L. Wu, J. X. Duan, H. T. Cao, Q. H. Zhang, L. Gu, L. F. Huang and Y. W. Cao, *Acs Appl Mater Inter*, 2021, **13**, 60182–60191.
9. A. A. Barragan, N. V. Ilawe, L. Zhong, B. M. Wong and L. Mangolini, *J Phys Chem C*, 2017, **121**, 2316-2322.
10. R. Rajeswarapalanichamy, G. S. Priyanga, M. Kavitha, S. Puvaneswari and K. Iyakutti, *Journal of Physics and Chemistry of Solids*, 2014, **75**, 888-902.

11. V. Adhikari, Z. T. Y. Liu, N. J. Szymanski, I. Khatri, D. Gall, P. Sarin and S. V. Khare, *Journal of Physics and Chemistry of Solids*, 2018, **120**, 197-206.

12. K. Balasubramanian, S. V. Khare and D. Gall, *Acta Mater*, 2018, **159**, 77-88.

13. G. M. Matenoglou, L. E. Koutsokeras, C. E. Lekka, G. Abadias, S. Camelio, G. A. Evangelakis, C. Kosmidis and P. Patsalas, *J Appl Phys*, 2008, **104**, 124907.

14. R. S. Ningthoujam and N. S. Gajbhiye, *Prog Mater Sci*, 2015, **70**, 50-154.

15. C. Freysoldt, B. Grabowski, T. Hickel, J. Neugebauer, G. Kresse, A. Janotti and C. G. Van de Walle, *Rev Mod Phys*, 2014, **86**, 253.

16. C. E. Ekuma, D. Bagayoko, M. Jarrell and J. Moreno, *Aip Adv*, 2012, **2,** 012189.

17. M. Fuchs, J. L. F. Da Silva, C. Stampfl, J. Neugebauer and M. Scheffler, *Phys Rev B*, 2002, **65,** 245212.

18. D. Holec, M. Friák, J. Neugebauer and P. H. Mayrhofer, *Phys Rev B*, 2012, **85**, 064101.

19. A. Pathak and A. K. Singh, *High Temp Mat Pr-Isr*, 2016, **35**, 389-398.

20. H. Hu and G. H. Peslherbe, *The Journal of Physical Chemistry C*, 2021, **125**, 8927-8937.

21. G. Tan, S. Hao, J. Zhao, C. Wolverton and M. G. Kanatzidis, *Journal of the American Chemical Society*, 2017, **139**, 6467-6473.

22. B. Medasani, M. Haranczyk, A. Canning and M. Asta, *Comp Mater Sci*, 2015, **101**, 96-107.

23. S. Mandal, K. Haule, K. M. Rabe and D. Vanderbilt, *npj Computational Materials*, 2019, **5**, 115.

24. B. O. Mnisi, *Bull. Mater Sci*, 2022, **45,** 16.

25. C. Stampfl and C. G. Van de Walle, *Phys Rev B*, 1999, **59**, 5521-5535.

26. P. Haas, F. Tran and P. Blaha, *Phys Rev B*, 2009, **79**, 085104.

27. P. Hohenberg and W. Kohn, *Physical Review*, 1964, **136**, B864-B871.

28. W. Kohn and L. J. Sham, *Physical Review*, 1965, **140**, A1133-A1138.

29. G. Kresse and J. Furthmuller, *Comp Mater Sci*, 1996, **6**, 15-50.

30. G. Kresse and J. Hafner, *Phys Rev B*, 1993, **48**, 13115-13118.

31. M. G. Quesne, A. Roldan, N. H. de Leeuw and C. R. A. Catlow, *Physical Chemistry Chemical Physics*, 2018, **20**, 6905-6916.

32. Z.-G. Mei, A. M. Yacout, Y. S. Kim, G. Hofman and M. Stan, *Journal of Nuclear Materials*, 2016, **471**, 208-213.

33. V. Petrman and J. Houska, *Journal of Materials Science*, 2013, **48**, 7642-7651.

34. G. X. Zhang, A. M. Reilly, A. Tkatchenko and M. Scheffler, *New J Phys*, 2018, **20,** 063020.

35. J. Greeley, T. F. Jaramillo, J. Bonde, I. Chorkendorff and J. K. Nørskov, *Nature Materials*, 2006, **5**, 909-913.

36. J. Greeley, I. E. L. Stephens, A. S. Bondarenko, T. P. Johansson, H. A. Hansen, T. F. Jaramillo, J. Rossmeisl, I. Chorkendorff and J. K. Nørskov, *Nature Chemistry*, 2009, **1**, 552-556.

37. Z. T. Y. Liu, X. Zhou, S. V. Khare and D. Gall, *Journal of Physics: Condensed Matter*, 2013, **26**, 025404.

38. D. Ologunagba and S. Kattel, *Energies*, 2020, **13**, 2182.

39. W. Sun, A. Holder, B. Orvañanos, E. Arca, A. Zakutayev, S. Lany and G. Ceder, *Chemistry of Materials*, 2017, **29**, 6936-6946.

40. H. B. Nie, S. Y. Xu, S. J. Wang, L. P. You, Z. Yang, C. K. Ong, J. Li and T. Y. F. Liew, *Applied Physics A*, 2001, **73**, 229-236.

41. A. F. Young, C. Sanloup, E. Gregoryanz, S. Scandolo, R. J. Hemley and H.-k. Mao, *Physical Review Letters*, 2006, **96**, 155501.

42. A. Costales, M. A. Blanco, Á. Martín Pendás, A. K. Kandalam and R. Pandey, *Journal of the American Chemical Society*, 2002, **124**, 4116-4123.

43. C. Giordano and M. Antonietti, *Nano Today*, 2011, **6**, 366-380.

44. J. L. Lyons and C. G. Van de Walle, *npj Computational Materials*, 2017, **3**, 12.

45. X. Yang, J. Nash, J. Anibal, M. Dunwell, S. Kattel, E. Stavitski, K. Attenkofer, J. G. Chen, Y. Yan and B. Xu, *Journal of the American Chemical Society*, 2018, **140**, 13387-13391.

46. Y. Abghoui, A. L. Garden, J. G. Howalt, T. Vegge and E. Skúlason, *ACS Catalysis*, 2016, **6**, 635-646.

47. T.-N. Ye, S.-W. Park, Y. Lu, J. Li, M. Sasase, M. Kitano and H. Hosono, *Journal of the American Chemical Society*, 2020, **142**, 14374-14383.

48. X. Yang, S. Kattel, J. Nash, X. X. Chang, J. H. Lee, Y. S. Yan, J. G. G. Chen and B. J. Xu, *Angew Chem Int Edit*, 2019, **58**, 13768-13772.

49. F. Tran and P. Blaha, *Phys. Rev. Lett.*, 2009, **102**, 226401.

50. P. Borlido, T. Aull, A. W. Huran, F. Tran, M. A. L. Marques, and S. Botti, *J. Chem. Theory Comput.* 2019, 15, 9, 5069–5079

Table of Content (TOC) Image

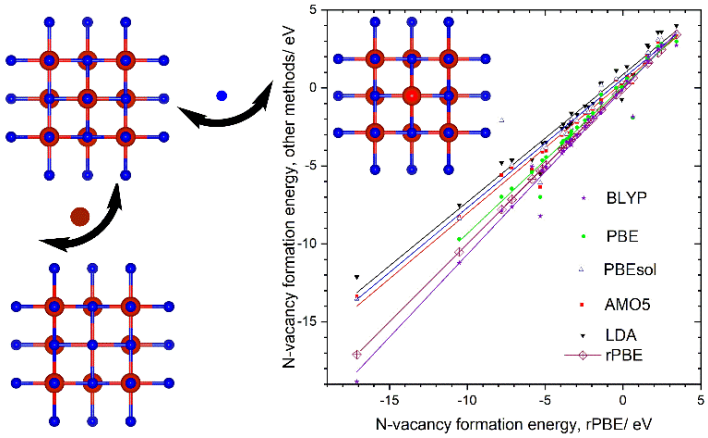

Bulk properties of transition metal nitrides, an emerging class of materials studied using various DFT exchange and correlation functionals.